

**Modeling of Microwave Multi-Frequency Backscatter and Emission of Land Surface by a Community Land Active Passive Microwave Radiative Transfer Modeling Platform (CLAP)**

Hong Zhao<sup>1</sup>, Yijian Zeng<sup>1</sup>, Jan G. Hofste<sup>1</sup>, Ting Duan<sup>1</sup>, Jun Wen<sup>2</sup>, Zhongbo Su<sup>1</sup>

1. Faculty of Geo-information Science and Earth Observation (ITC), University of Twente, 7514 AE, Enschede, The Netherlands ([h.zhao@utwente.nl](mailto:h.zhao@utwente.nl))
2. College of Atmospheric Sciences, Plateau Atmosphere and Environment Key Laboratory of Sichuan Province, Chengdu University of Information Technology, Chengdu, China

**Estimated vegetation water content (VWC)**

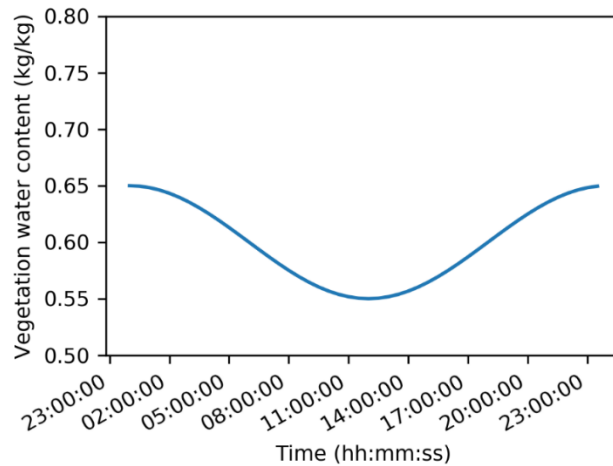


Figure S1 Estimated vegetation water content using the sinusoidal function with the aid of *in situ* observations.

**Noise level data**

Table S1 Calculated noise floor over the different frequencies under different polarizations.

Band	Polarization	Wx	Wy	A <sup>sq</sup>	A <sup>sq</sup> *0.9	A <sup>sq</sup> *0.8	sigma_min (dB)	sigma_min/A <sup>sq</sup> *0.9	sigma_min/A <sup>sq</sup> *0.8	sigma_min/A <sup>sq</sup> *0.8 (power ratio)
L	vv	5.	4.	26.	23.5	21.0	-53	-67	-66	2.0E-07
		5.	4.	23.	21.5	19.1	-49	-62	-62	6.3E-07
		5.	3.	21.	19.5	17.3	-53	-66	-65	2.5E-07
S	vh	4.	4.	18.	16.4	14.6	-52	-64	-64	4.0E-07
		4.	3.	16.	14.8	13.2	-51	-63	-62	5.0E-07
		85	4	5	14.8	13.2	-51	-63	-62	5.0E-07

	hh	5.	2.	14.	12.8	11.4	-54	-64	-65	3.2E-07
C	vv	4.	2.		8.9	7.8	-51	-60	-60	1.0E-06
	vh	3.	2.		8.9	8	-51	-60	-60	1.0E-06
	hh	2.	10.		9.4	8.3	-52	-62	-61	6.3E-07
	hh	4	6	4	9.4	8.3	-52	-62	-61	6.3E-07
X	vv	2.	1.		2.4	2.1	-48	-52	-51	6.3E-06
	vh	2.	1.		2.6	2.3	-49	-53	-53	5.0E-06
	hh	2.	1.		2.6	2.3	-50	-54	-54	4.0E-06
	hh	05	4	2.9	2.6	2.3	-50	-54	-54	4.0E-06

\*where the values of  $\sigma_{\min}$  (dB) are those listed in Table E1 from (Hofste et al., 2021). The coefficient 0.8 in the term of  $\sigma_{\min}/A^{\text{sq}}*0.8$  is the transformation coefficient (i.e.,  $\pi/4$ ) from the rectangular area ( $4*W_x*W_y$ ) to the elliptical area ( $\pi*W_x*W_y$ ).

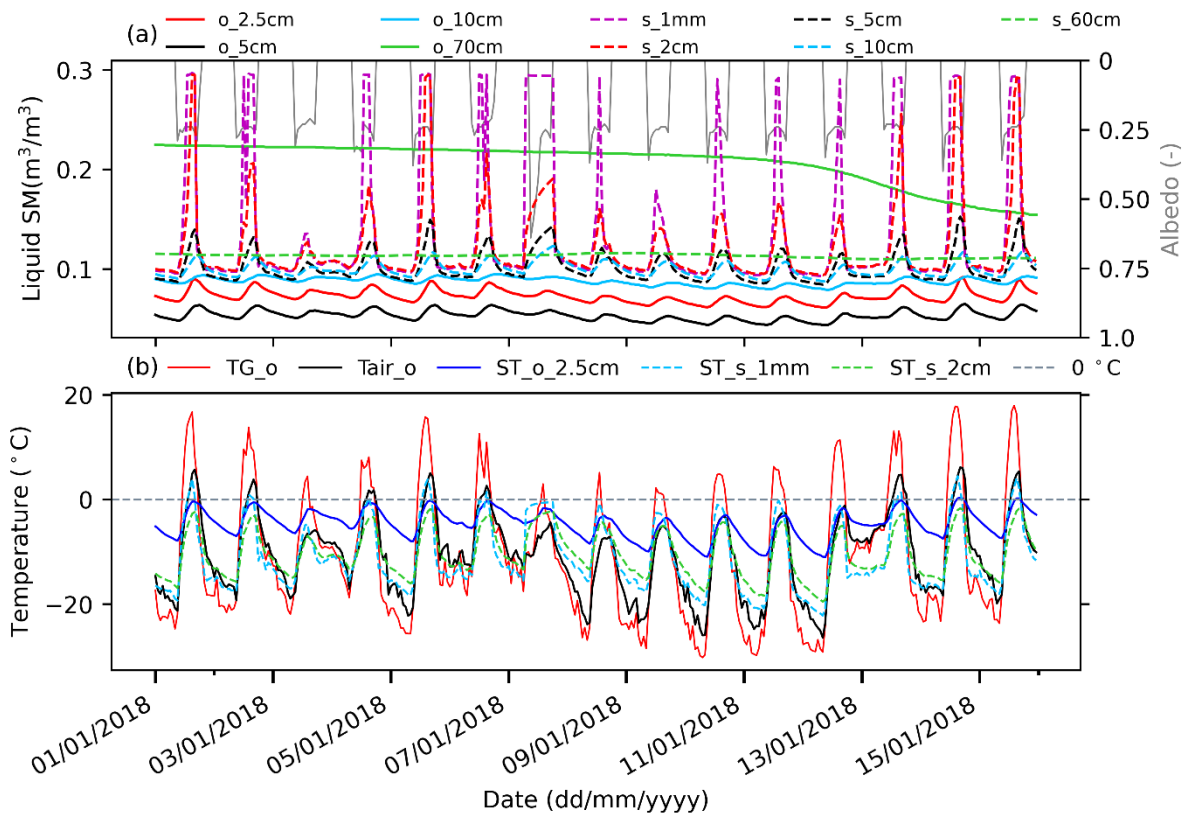


Figure S2 Plot of the *in situ* measured (*\_o*) soil variables, environmental variables and the STEMMUS simulated (*\_s*) soil moisture and temperature during the winter period. TG refers to ground surface temperature and Tair represents air temperature at 2 m.

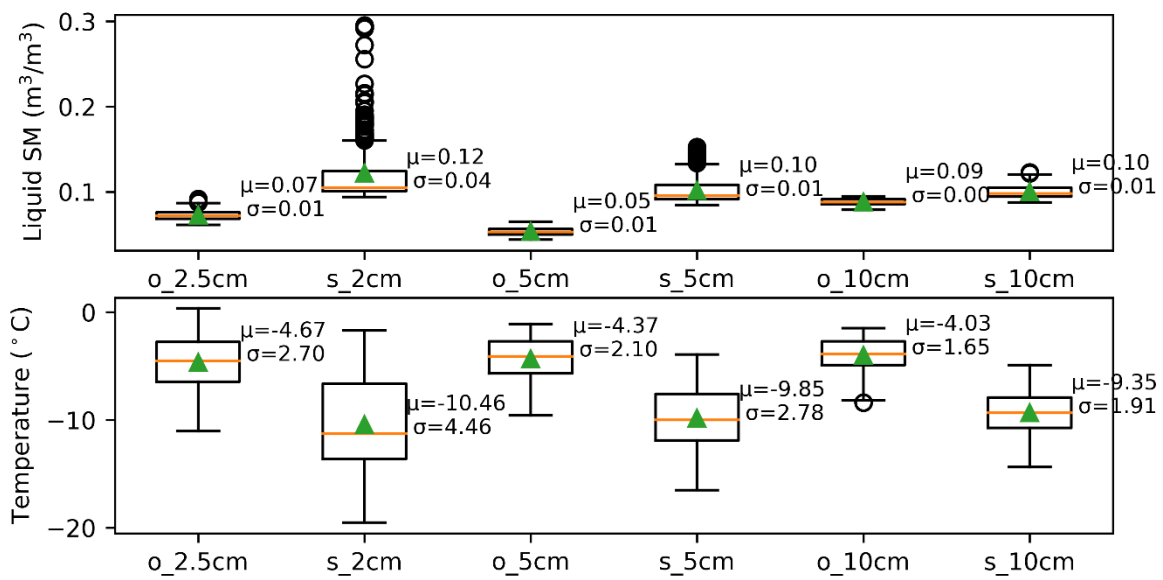


Figure S3 Boxplots of the *in situ* measured (o) soil moisture and temperature at the different depths (i.e., 2.5 cm, 5 cm and 10 cm) and the STEMMUS simulated (s) soil moisture and temperature at different depths during the same period as in Figure S2-1. The orange line denotes the mean ( $\mu$ ) value, and  $\sigma$  denotes the standard deviation. As shown in Figure S2-1, STEMMUS provides high values of liquid soil moisture at noon due to soil thaw process consideration in the model, and these high values are also observed as whiskers shown in Figure S2-2.

### Impact of dynamic vegetation temperature and VWC on the simulation of $\sigma_{pq}^0$ at multi-frequency

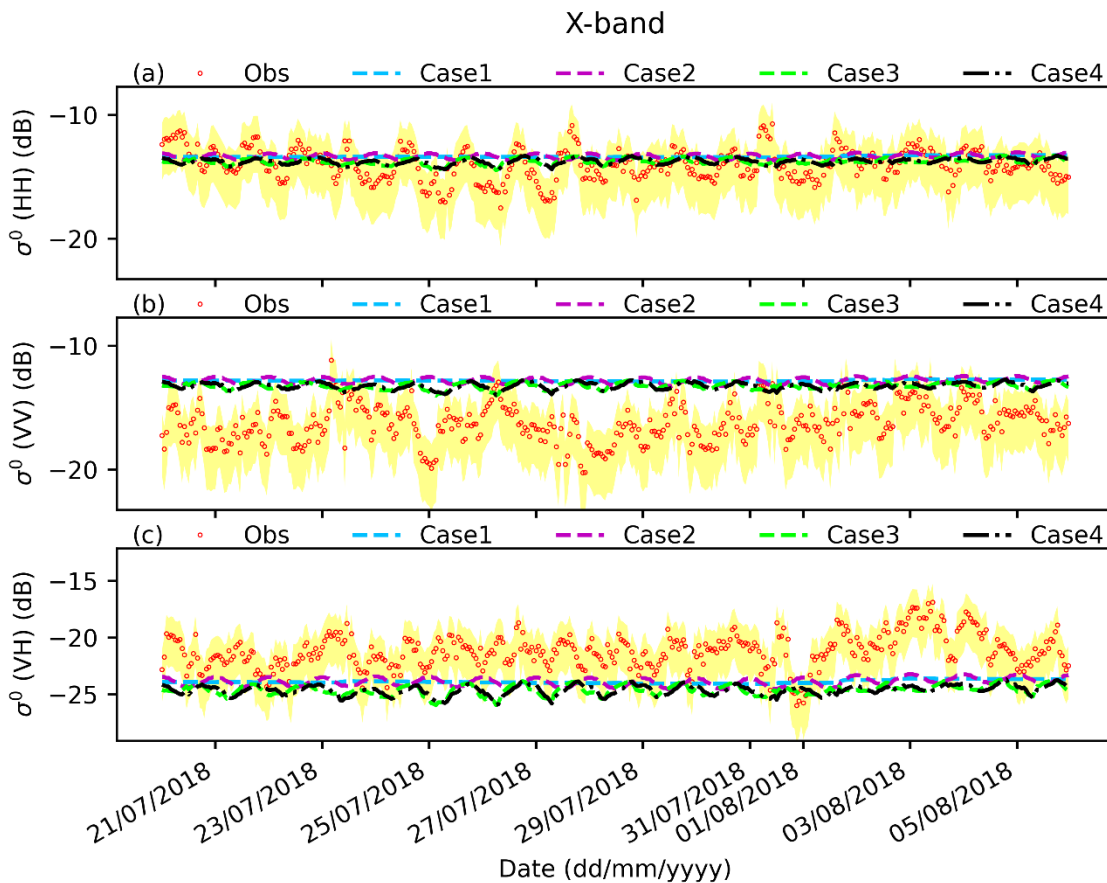


Figure S4  $\sigma_{pq}^0$  at the X-band simulated by the CLAP (ATS\_AIEM\_TVG model) with the disc parameterization using three different cases of vegetation temperature and VWC, compared to the ground-based observations during the summer period. Case 1 refers to the constant vegetation

temperature (20°) and VWC (0.6 kg/kg). Case 2 refers to constant vegetation temperature (20°) but estimated dynamic VWC (Figure S1). Case 3 refers to dynamic vegetation temperature (i.e., in-situ measured air temperature at 2 m) but constant VWC (0.6 kg/kg). Case 4 refers to the dynamic vegetation temperature used in Case 3 and the estimated dynamic VWC (Figure S1). The yellow shaded area refers to the uncertainty in the observed backscatter data (please see Hofste et al. (2021)).

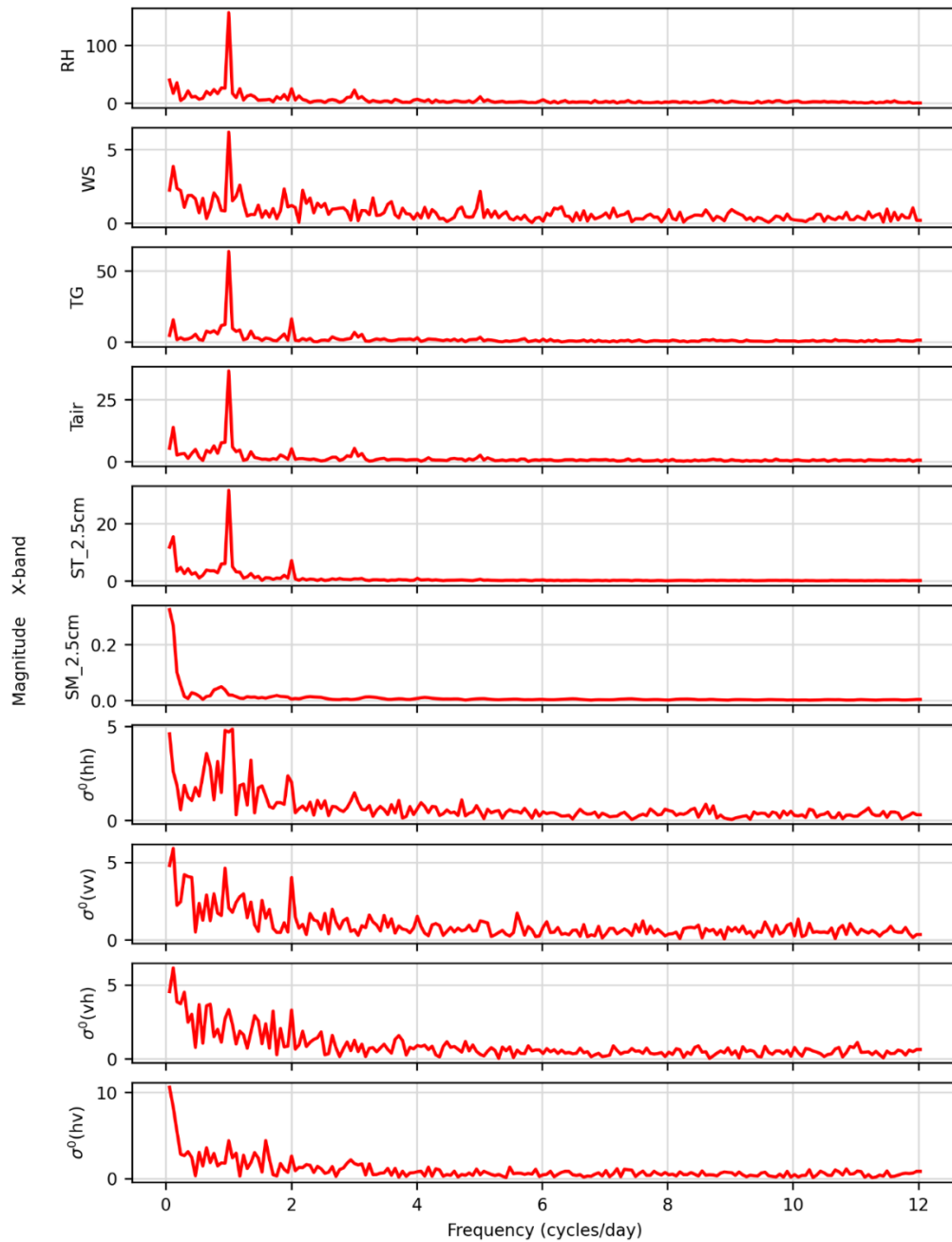


Figure S5 The *in situ* observed  $\sigma_{pq}^0$  at the X-band, environmental variables and soil state variables during the summer period analysed in the Frequency domain by the Fast Fourier transform algorithm. RH denotes relative humidity (%), WS denotes wind speed (m/s), TG refers to ground surface temperature (°C), Tair represents air temperature (°C) at 2 m, and SM\_2.5cm and ST\_2.5cm denote soil moisture and temperature respectively at 2.5 cm.

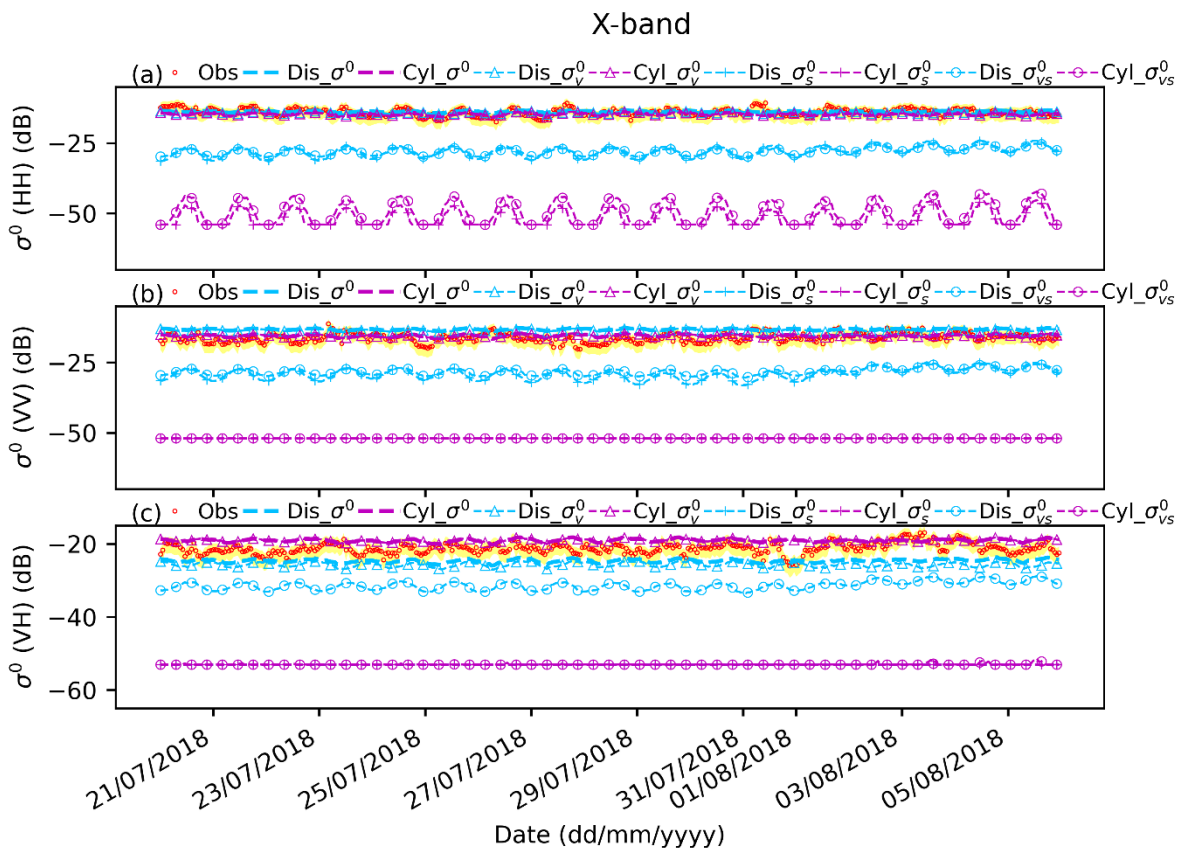


Figure S6  $\sigma_{pq}^0$  at the X-band and its components simulated by the CLAP (ATS\_AIEM\_TVG model) with the disc and cylinder parameterizations, compared to the ground-based observations during the summer period. Dis and Cyl refer to the disc and cylinder parameterizations respectively, and  $\sigma^0$ ,  $\sigma_v^0$ ,  $\sigma_s^0$  and  $\sigma_{vs}^0$  represent total, vegetation, soil and the interaction between vegetation and soil surface. The yellow shaded area refers to the uncertainty in the observed backscatter data (please refer to Hofste et al. (2021)).

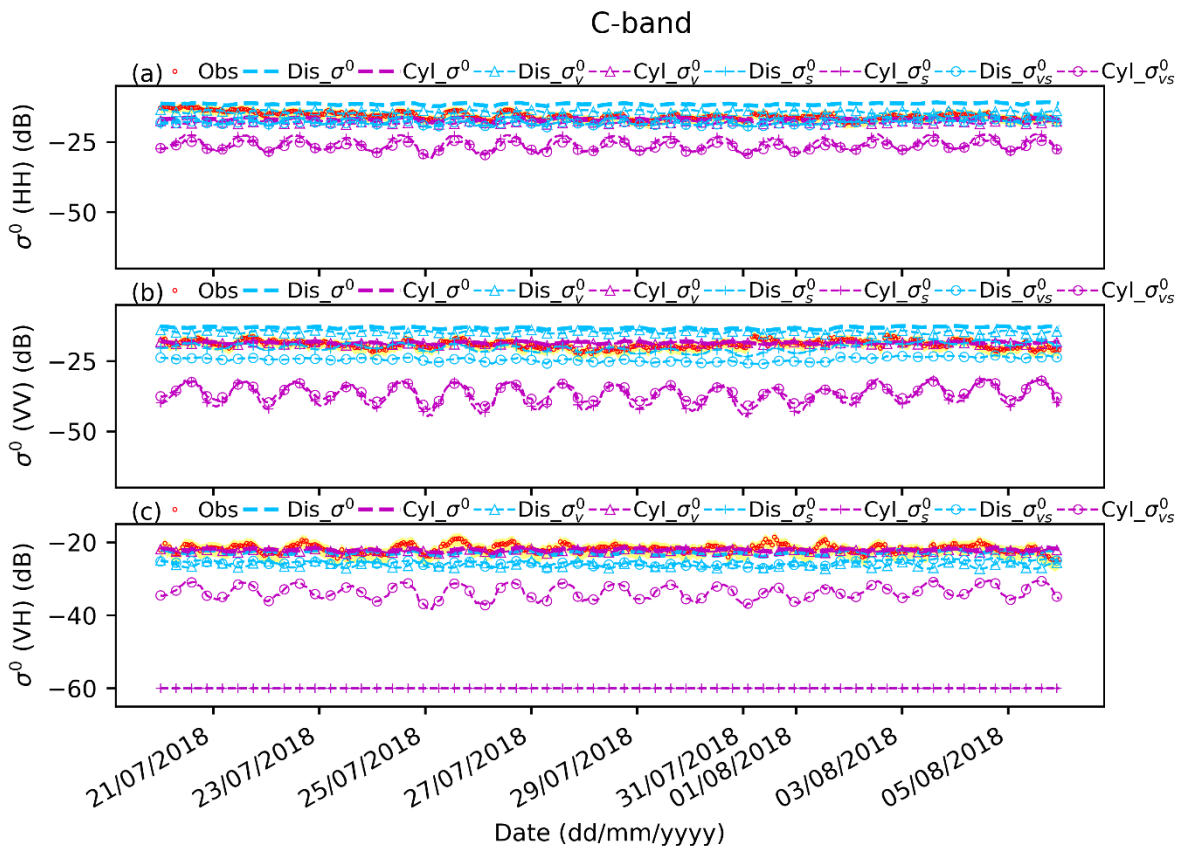


Figure S7 Same as Figure S6 but for C-band.

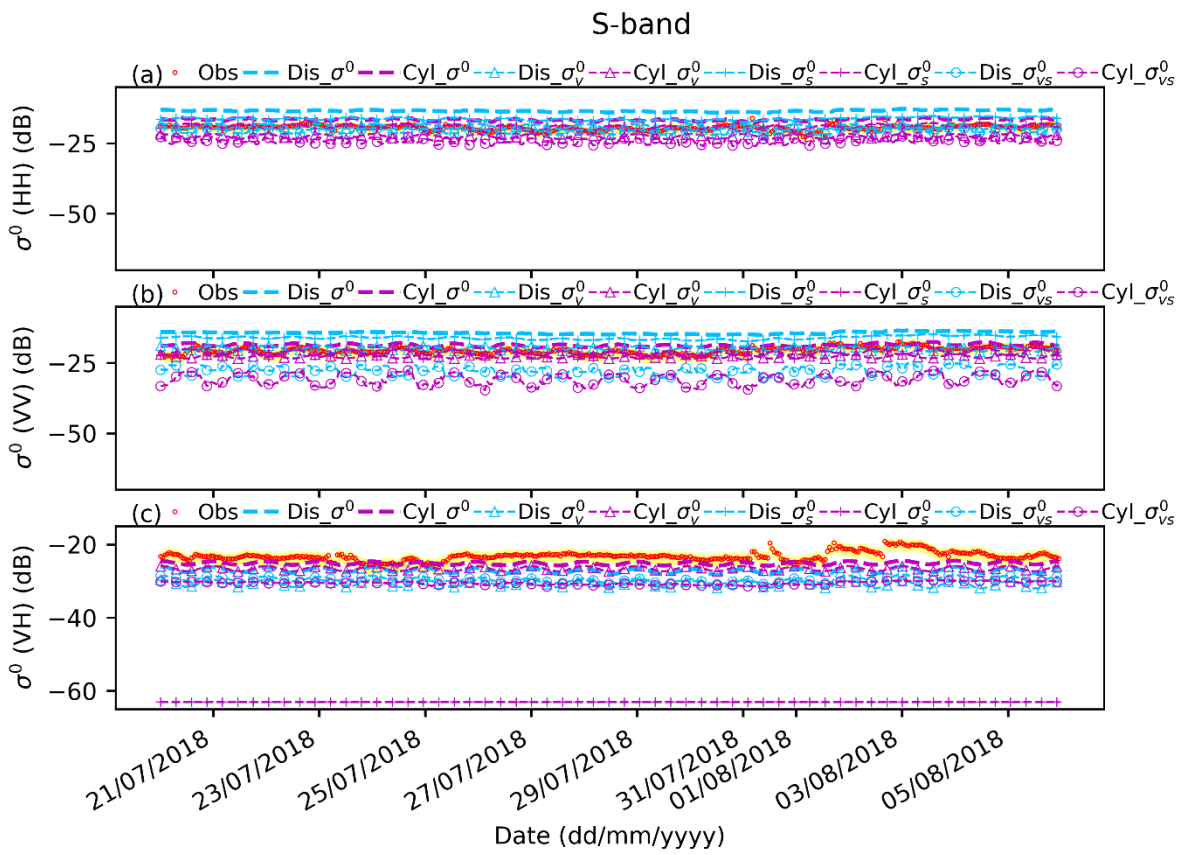


Figure S8 Same as Figure S6 but for S-band.

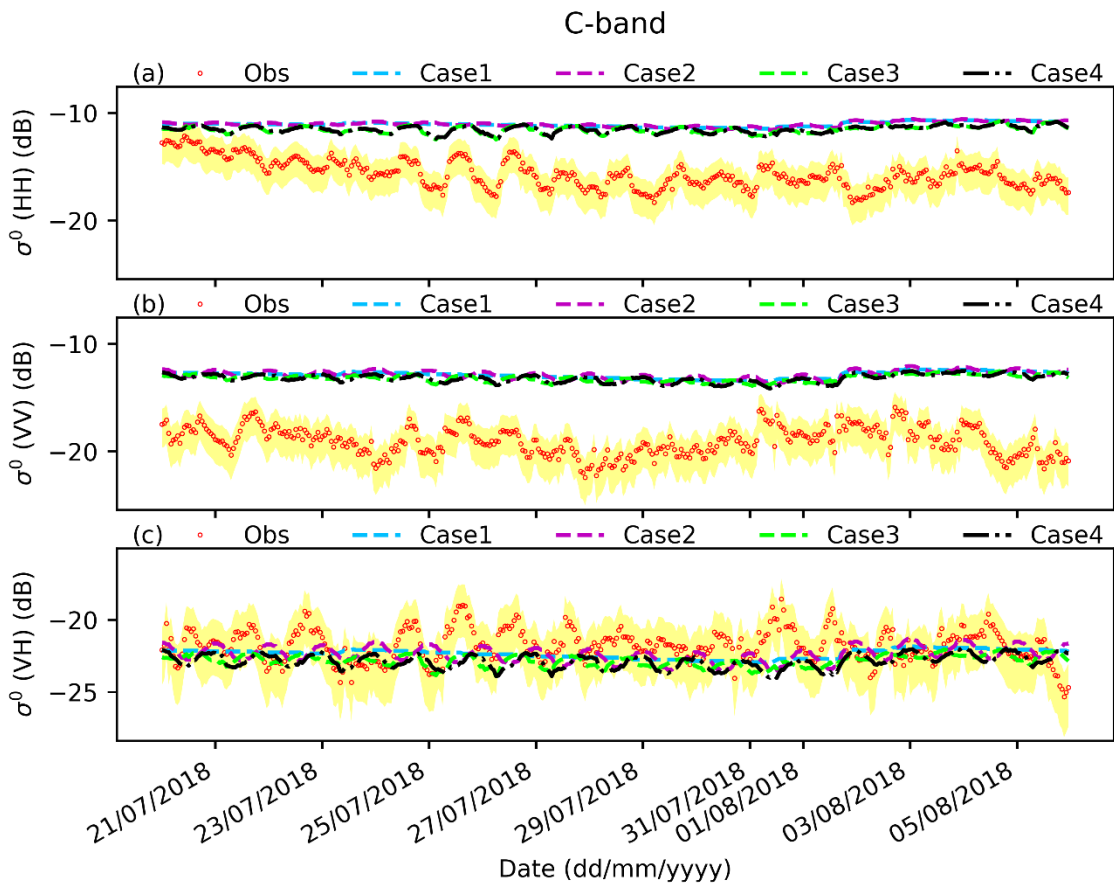


Figure S9  $\sigma_{pq}^0$  at the C-band simulated by the CLAP (ATS\_AIEM\_TVG model) with the disc parameterization using three different cases of vegetation temperature and VWC, compared to the ground-based observations during the summer period. Case 1 refers to the constant vegetation temperature ( $20^\circ$ ) and VWC (0.6 kg/kg). Case 2 refers to constant vegetation temperature ( $20^\circ$ ) but estimated dynamic VWC (Figure S1). Case 3 refers to dynamic vegetation temperature (i.e., in-situ measured air temperature at 2 m) but constant VWC (0.6 kg/kg). Case 4 refers to the dynamic

vegetation temperature used in Case 3 and the estimated dynamic VWC (Figure S1). The yellow shaded area refers to the uncertainty in the observed backscatter data (please see Hofste et al. (2021)).

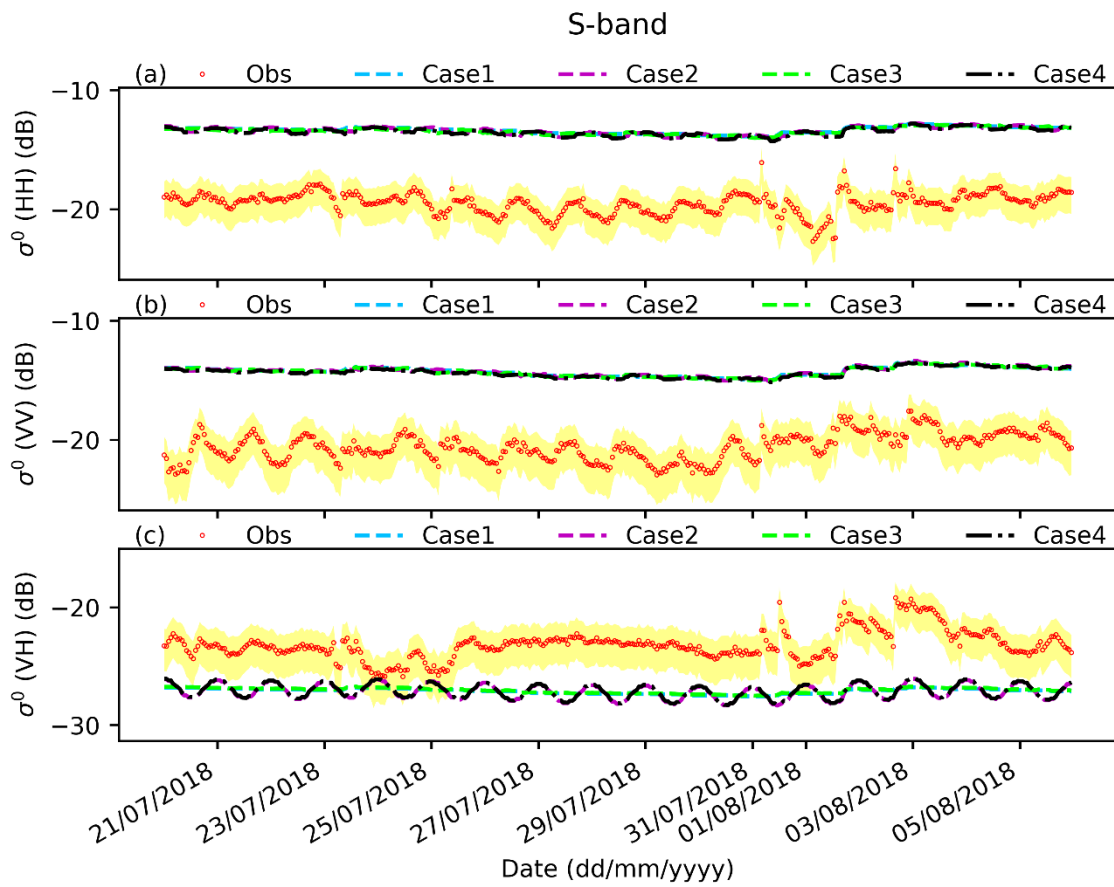


Figure S10 Same as Figure S9 but for S-band.

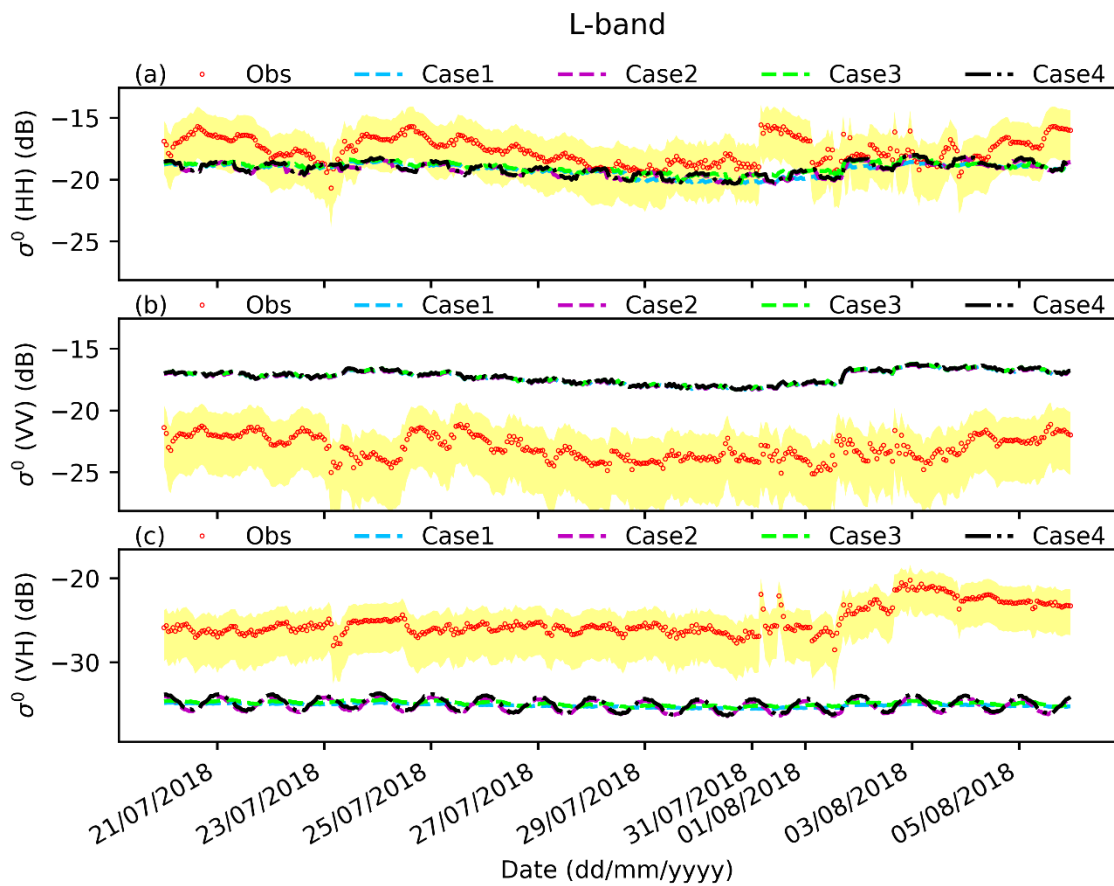


Figure S11 Same as Figure S9 but for L-band.

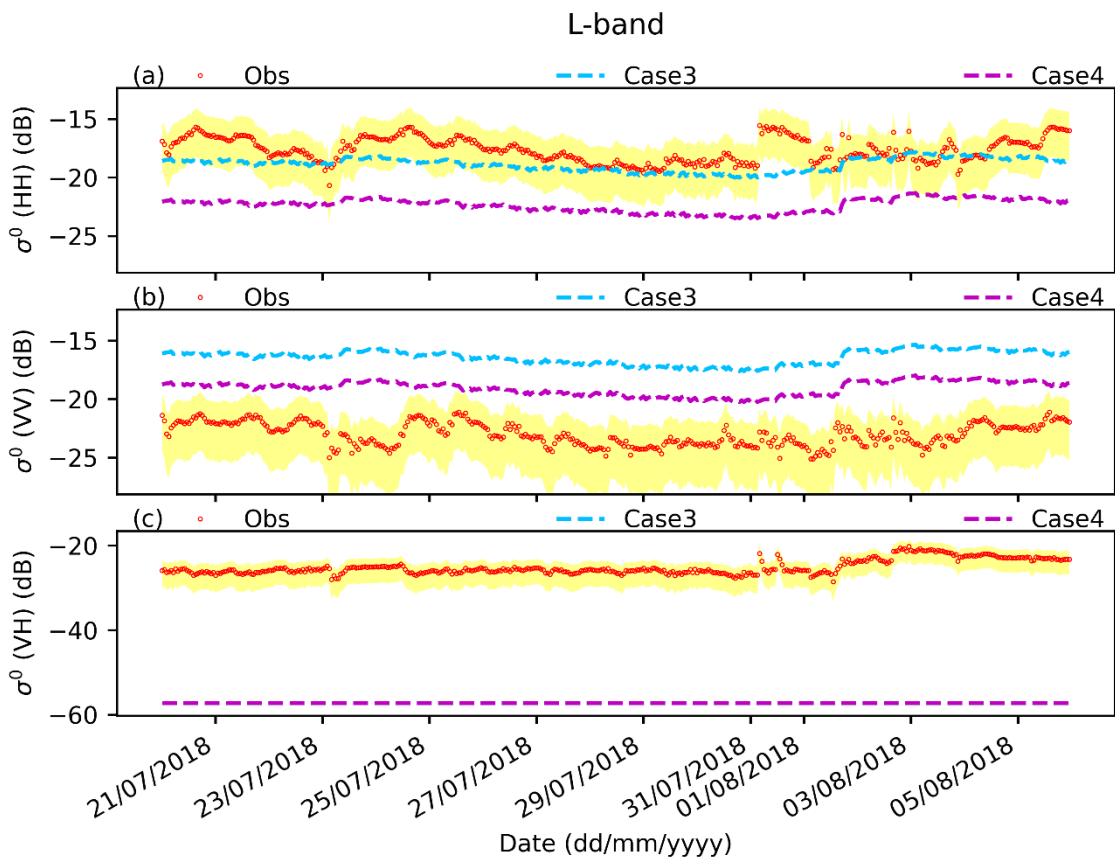


Figure S12 Same as Figure S9 but based on the cylinder parameterization.

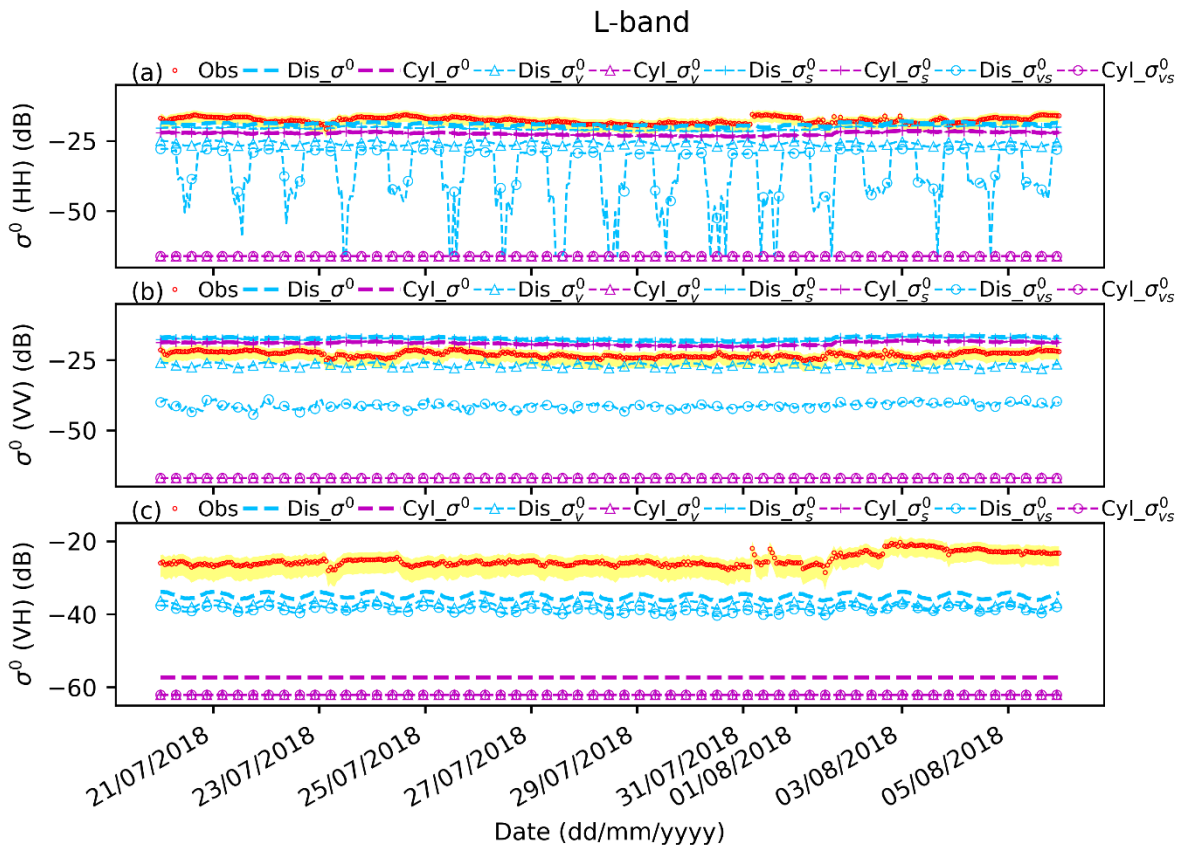


Figure S13  $\sigma_{pq}^0$  at the L-band and its components simulated by the CLAP (ATS\_AIEM\_TVG model) with the disc and cylinder parameterizations, compared to the ground-based observations during the summer period. Dis and Cyl refer to the disc and cylinder parameterizations respectively, and  $\sigma^0$ ,  $\sigma_v^0$ ,  $\sigma_s^0$  and  $\sigma_{vs}^0$  represent total, vegetation, soil and the interaction between vegetation and soil surface. The yellow shaded area refers to the uncertainty in the observed backscatter data (please refer to Hofste et al. (2021)).

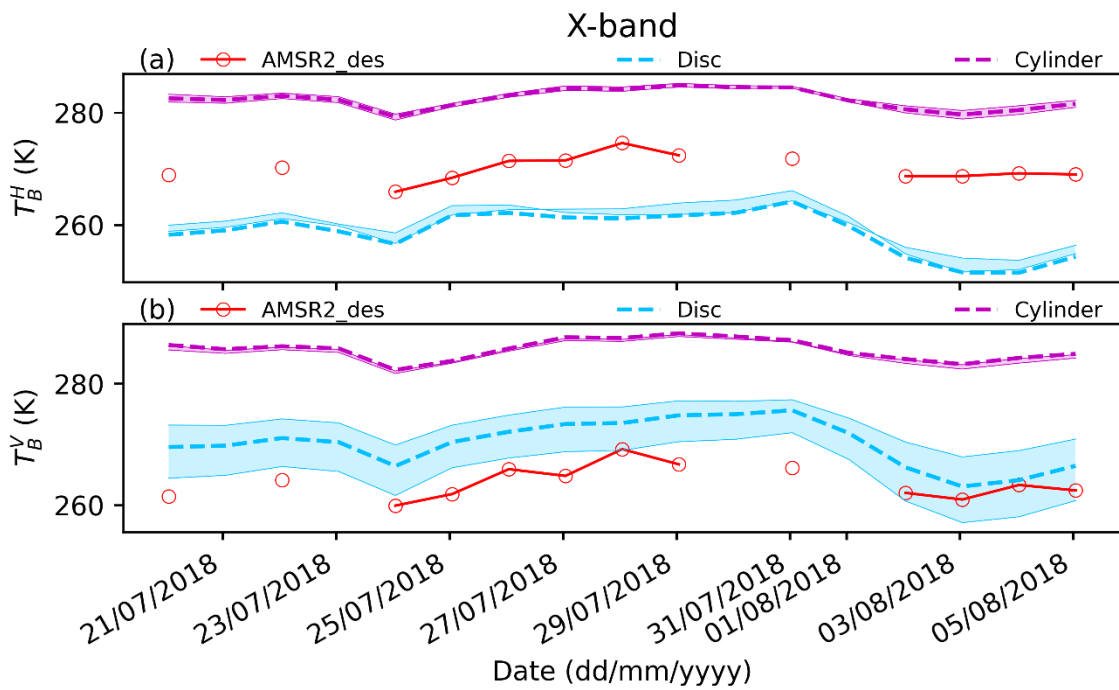


Figure S14  $T_B^p$  at the X-band simulated by the CLAP with the disc and cylinder parameterizations compared to the AMSR2 observations at the descending mode (local time: 1:30 am) during the summer period. Similar as in Figure 3 in the text, the shaded area overlapping the simulation results refers to the uncertainty due to the effect of the footprint area determined by the different incidence angles (please refer to Table 1 in the text).

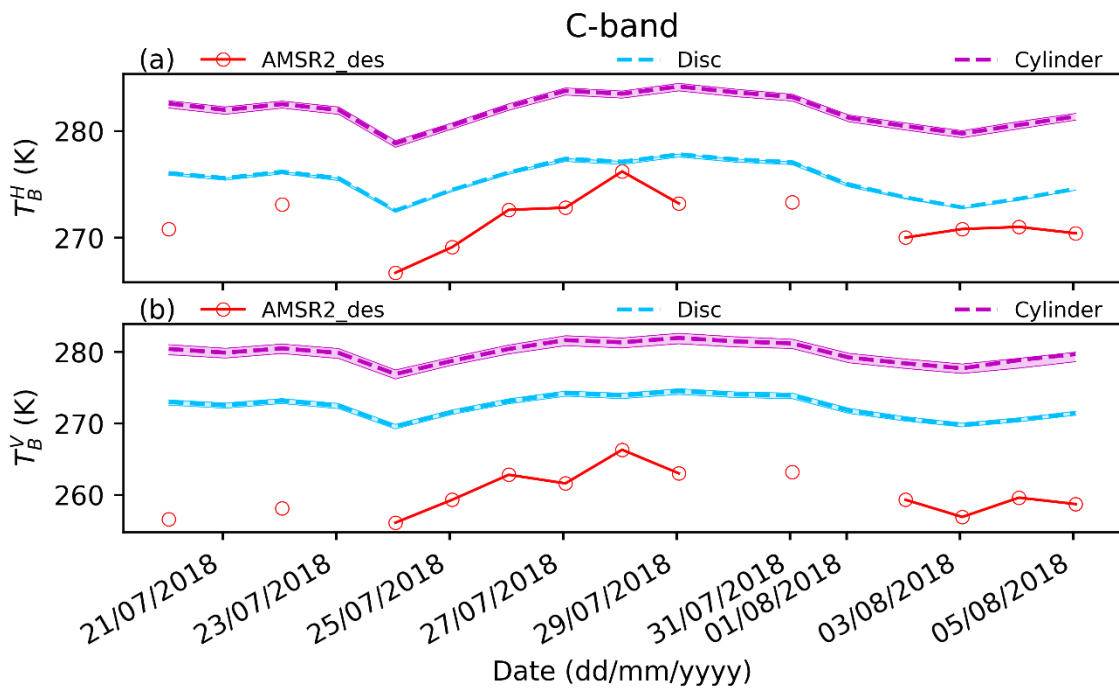


Figure S15 Same as Figure S14 but for C-band.

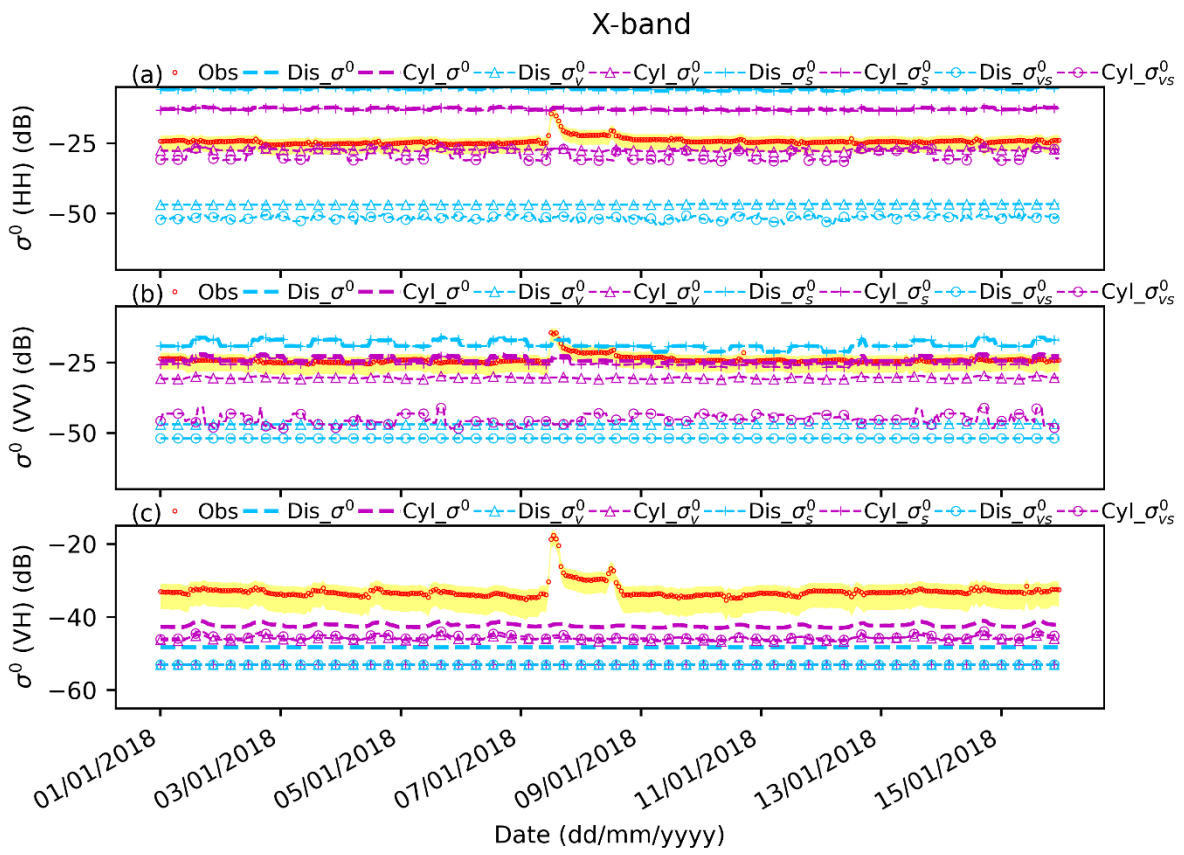


Figure S16  $\sigma_{pq}^0$  at the X-band and its components simulated by the CLAP (ATS\_AIEM\_TVG model) with the disc and cylinder parameterizations, compared to the ground-based observations during the winter period. Dis and Cyl refer to the disc and cylinder parameterizations respectively, and  $\sigma^0$ ,  $\sigma_v^0$ ,  $\sigma_s^0$  and  $\sigma_{vs}^0$  represent total, vegetation, soil and the interaction between vegetation and soil surface. The yellow shaded area refers to the uncertainty in the observed backscatter data (please refer to Hofste et al. (2021)).

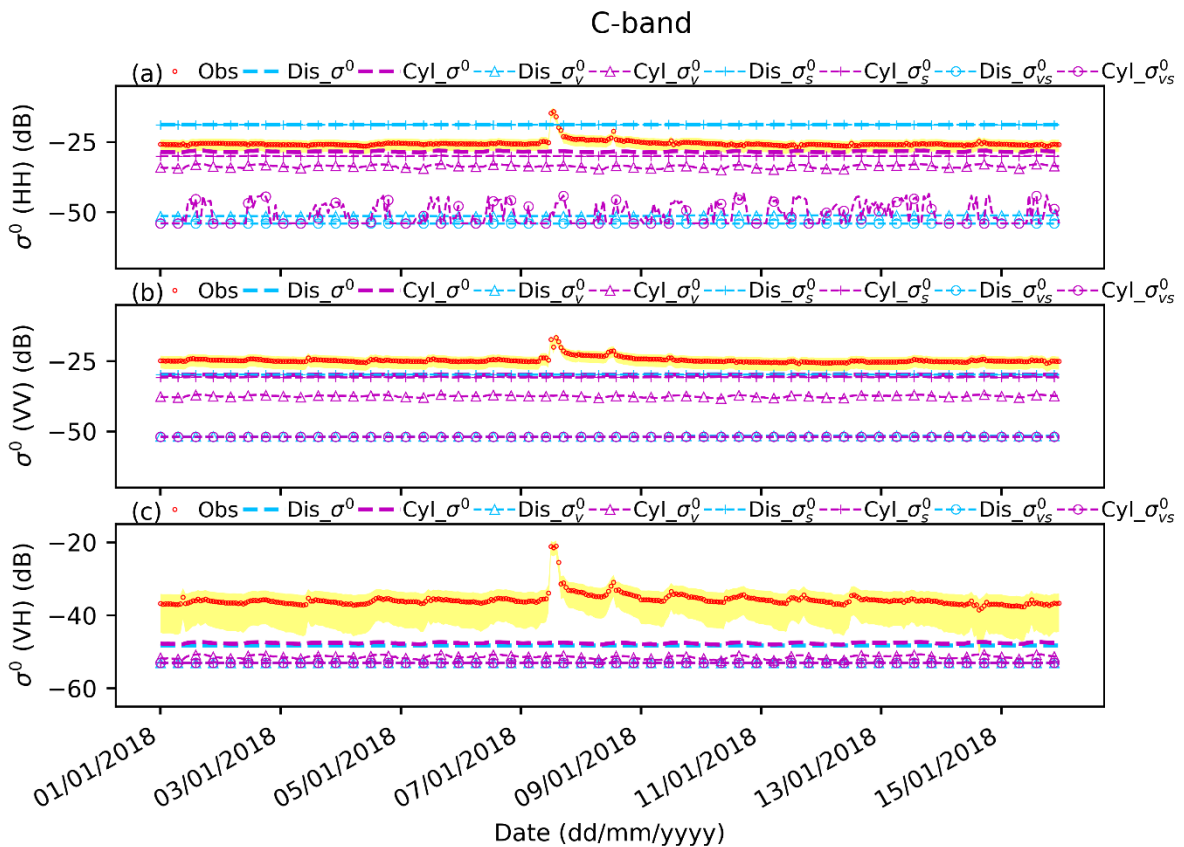


Figure S17 Same as Figure S16 but for X-band.

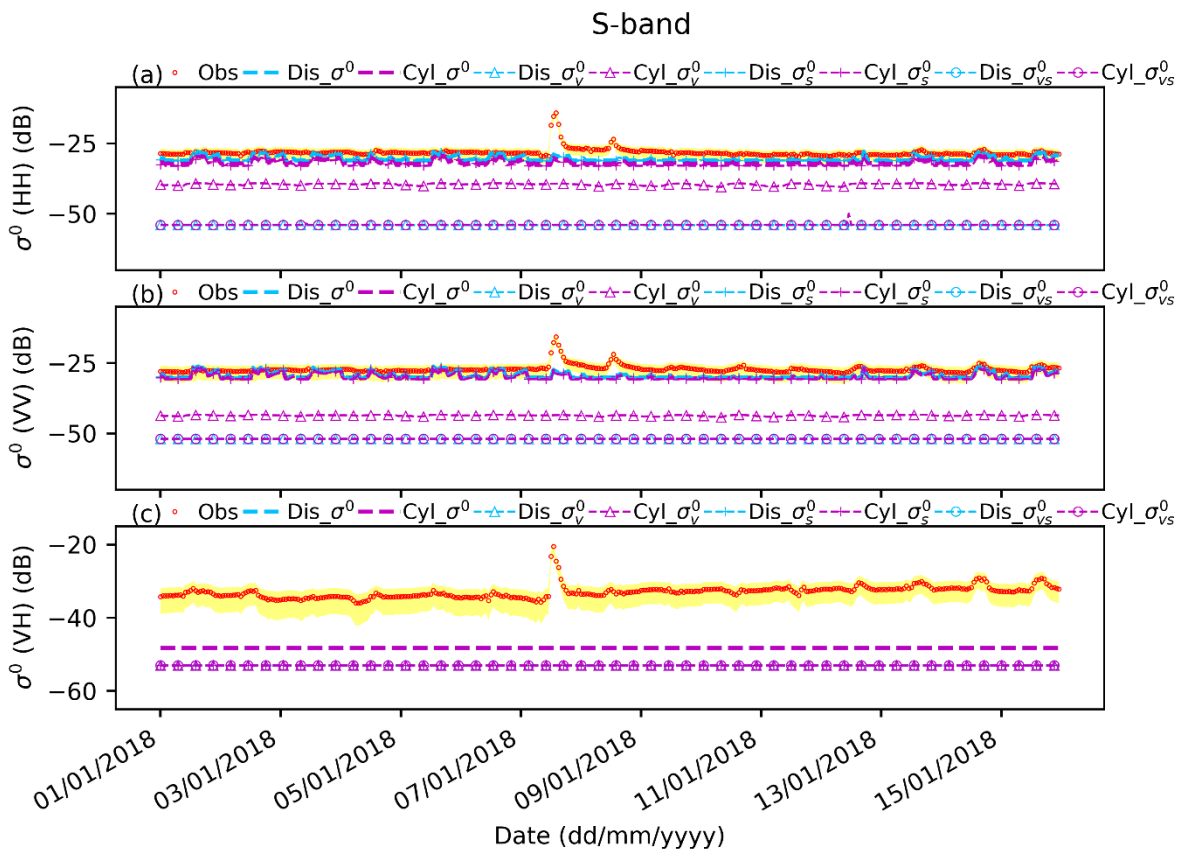


Figure S18 Same as Figure S16 but for the winter period.

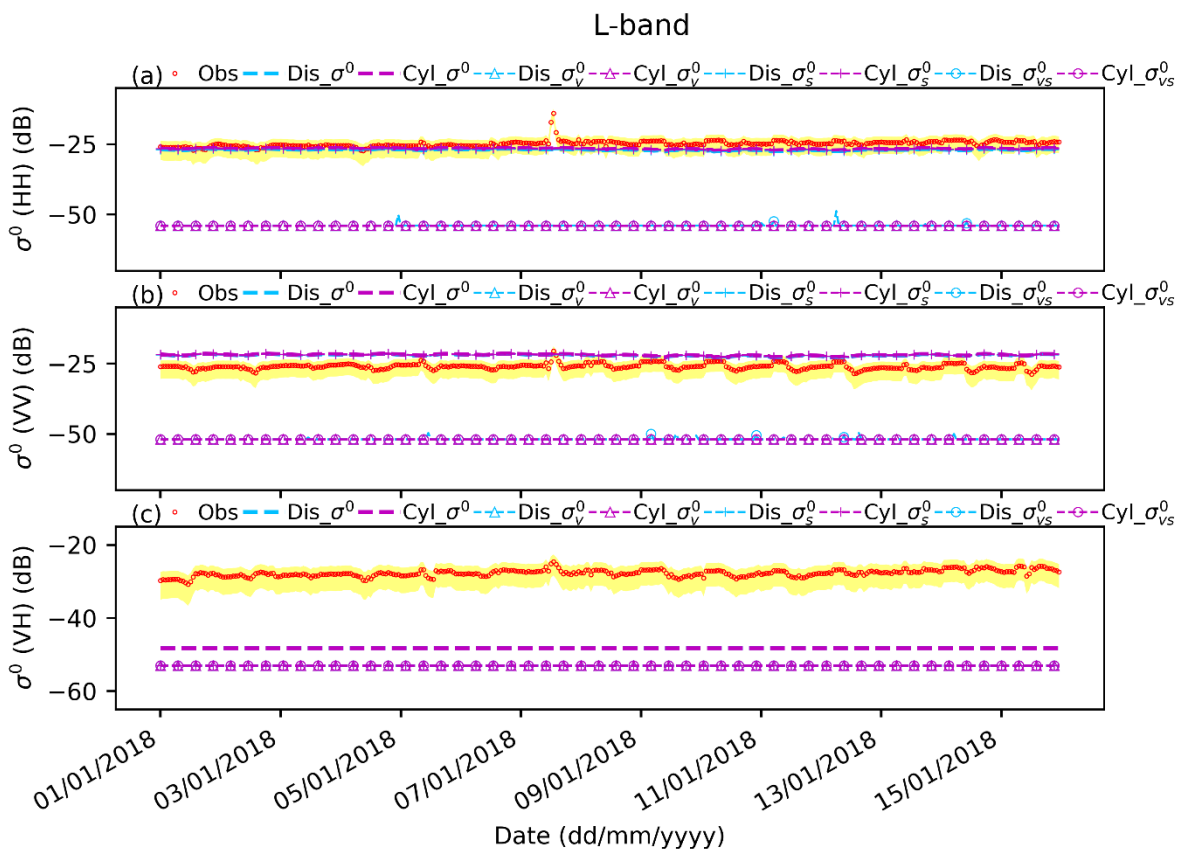


Figure S19 Same as Figure S16 but for the winter period.

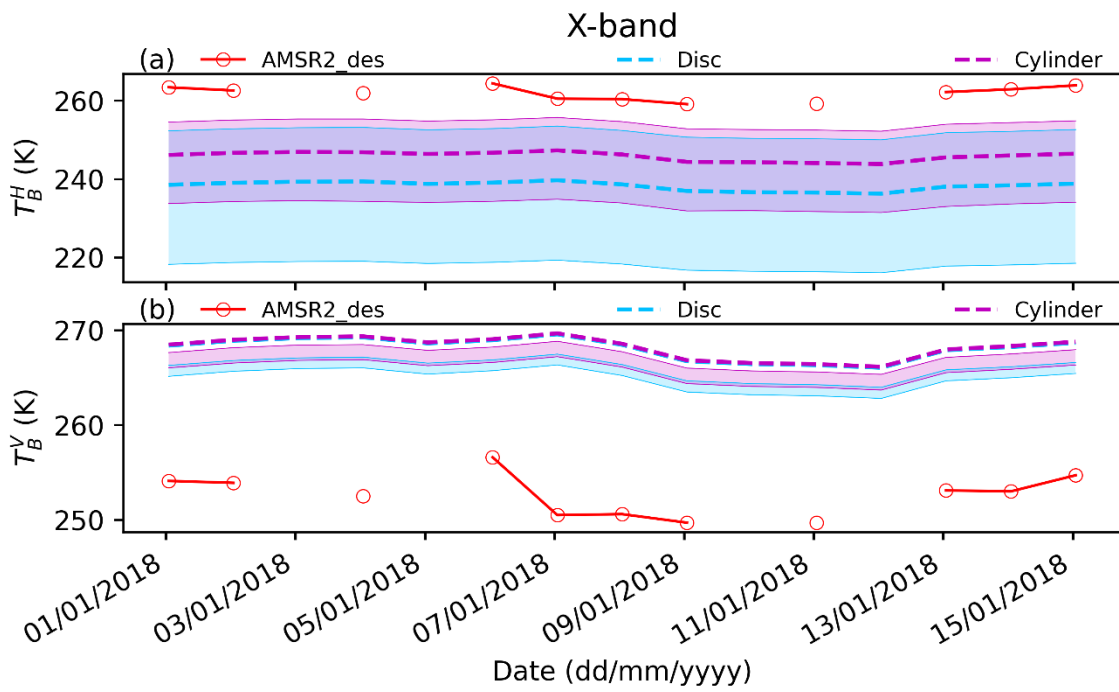


Figure S20  $T_B^p$  at the X-band simulated by the CLAP with the disc and cylinder parameterizations compared to the AMSR2 observations at the descending mode (local time: 1:30 am) during the winter period.

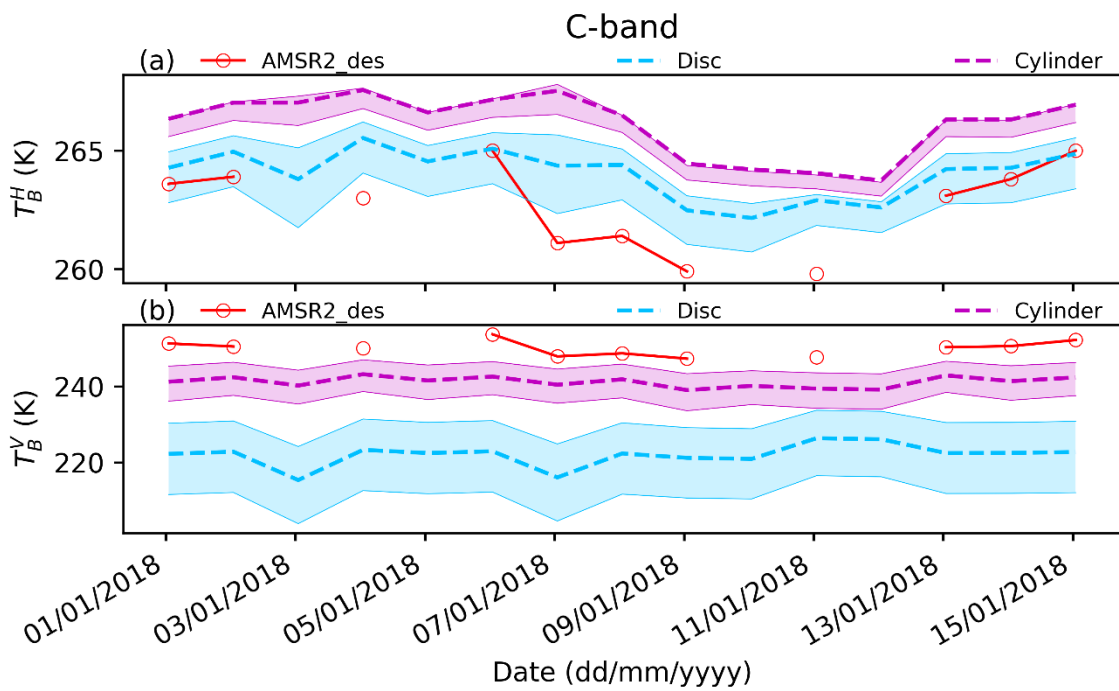


Figure S21 Same as Figure S20 but for C-band.

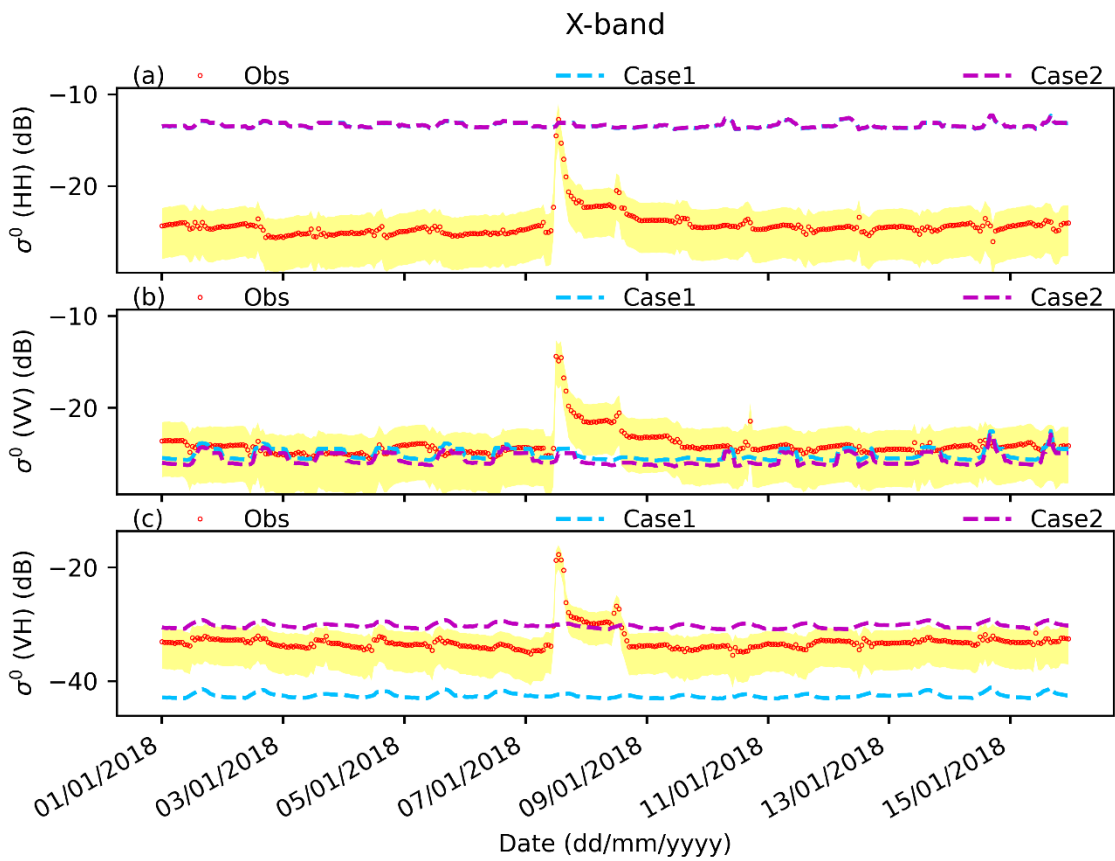


Figure S22  $\sigma_{pq}^0$  at the X-band simulated by the CLAP (ATS\_AIEM\_TVG model) with the cylinder parameterization using the different orientation of vegetation, compared to the ground observations during the winter period. Case 1 refers to the totally horizontal orientation of vegetation represented by beta angle of  $90^\circ$ . Case 2 refers to the tilted orientation of vegetation represented by beta angle ranging from  $60^\circ$  to  $90^\circ$ .

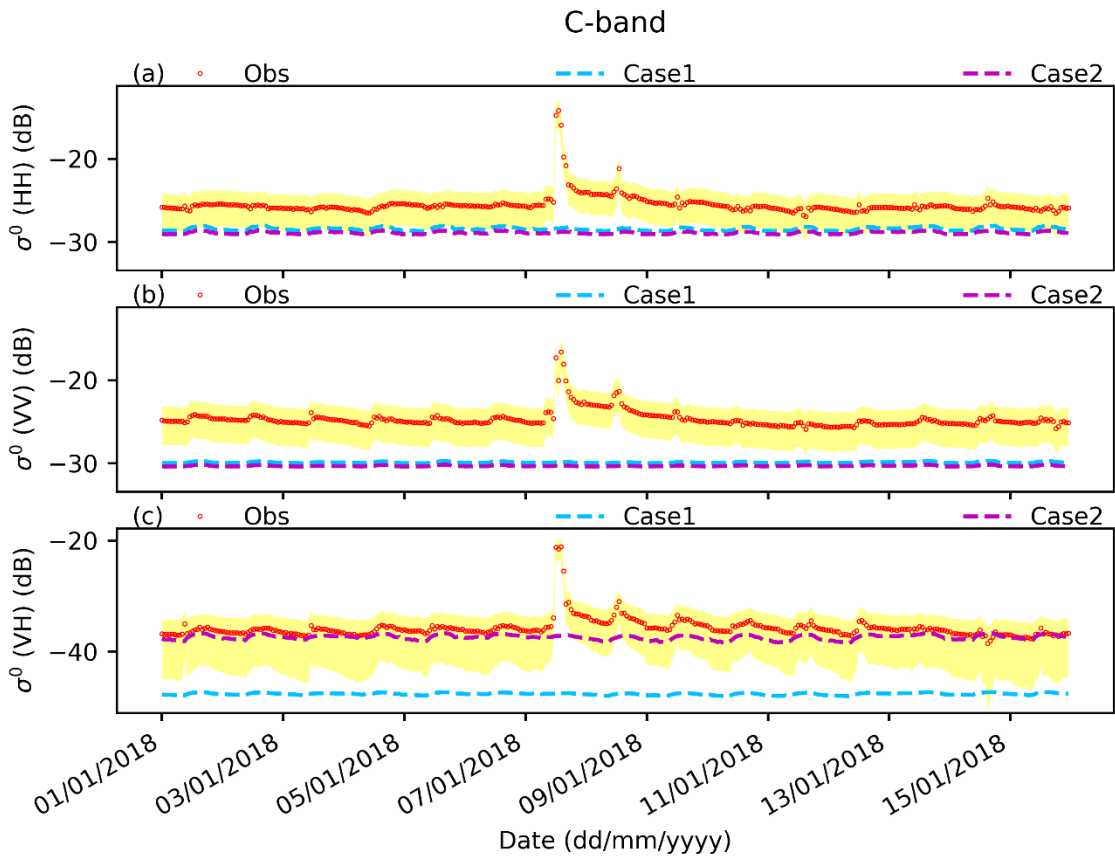


Figure S23 Same as Figure S22 but for C-band.

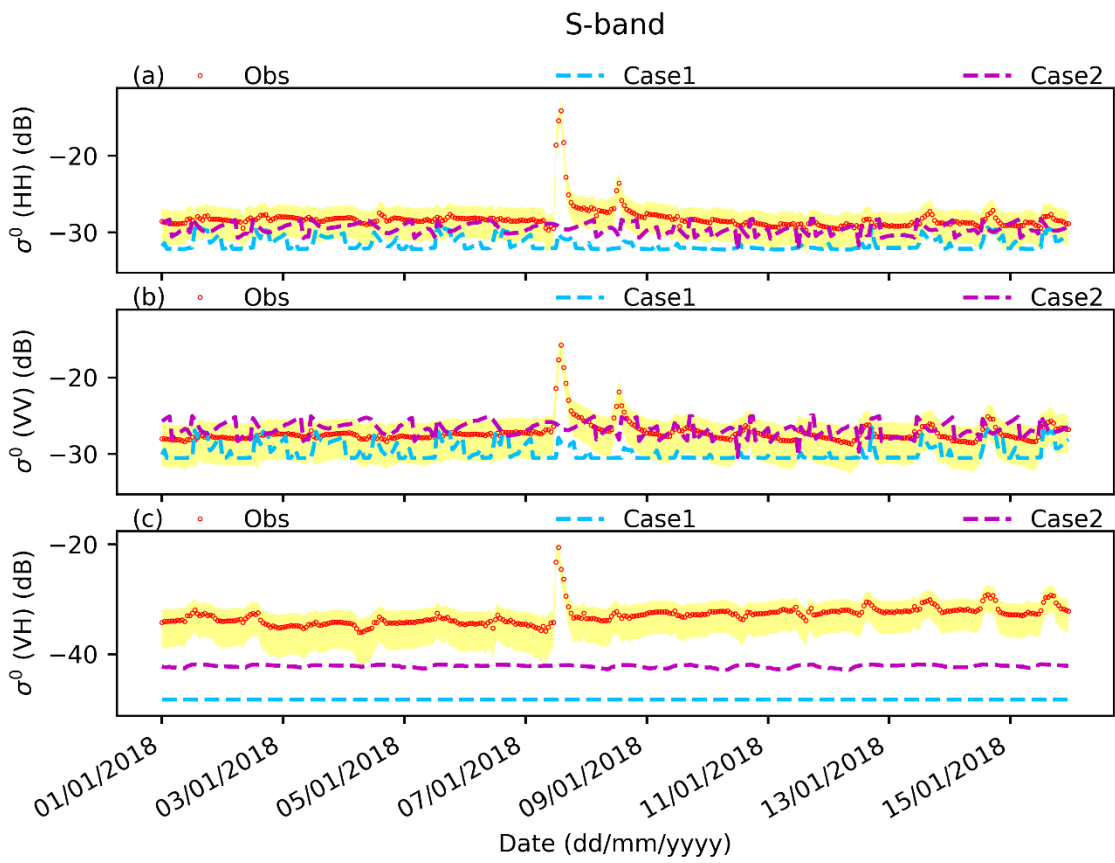


Figure S24 Same as Figure S22 but for S-band.

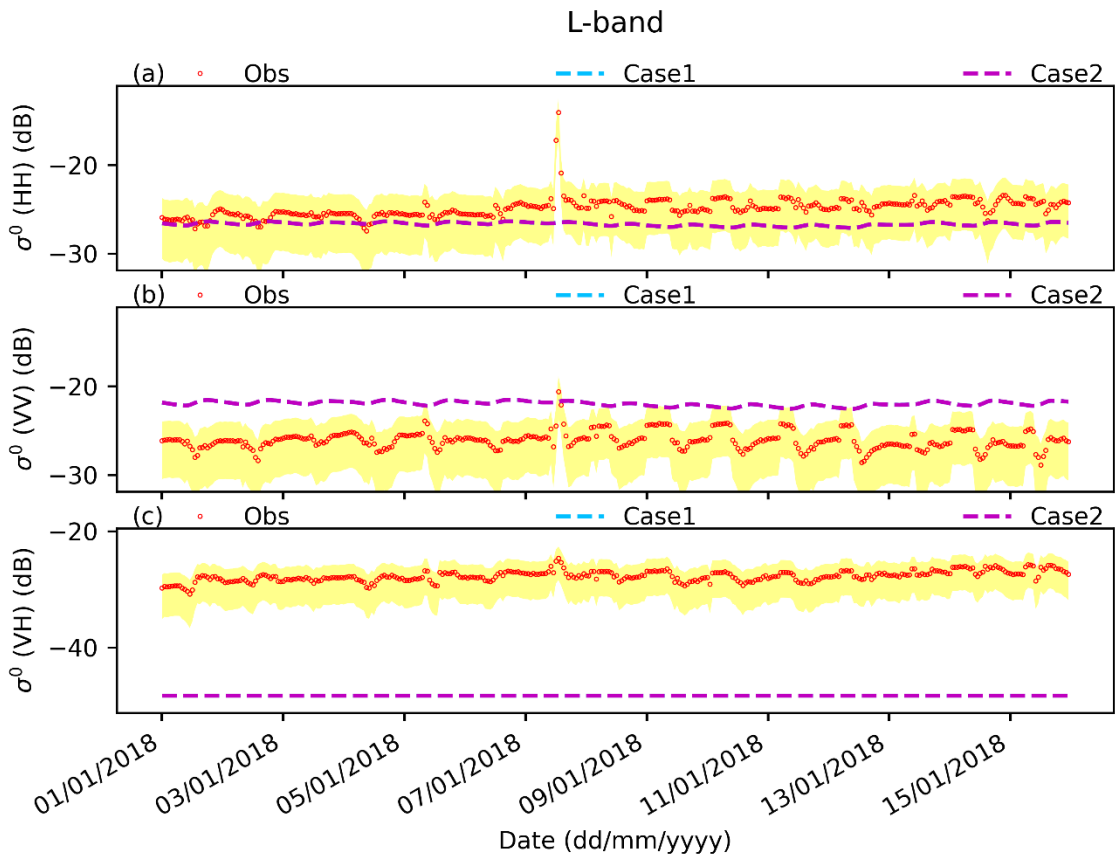


Figure S25 Same as Figure S22 but for L-band.

## L-band

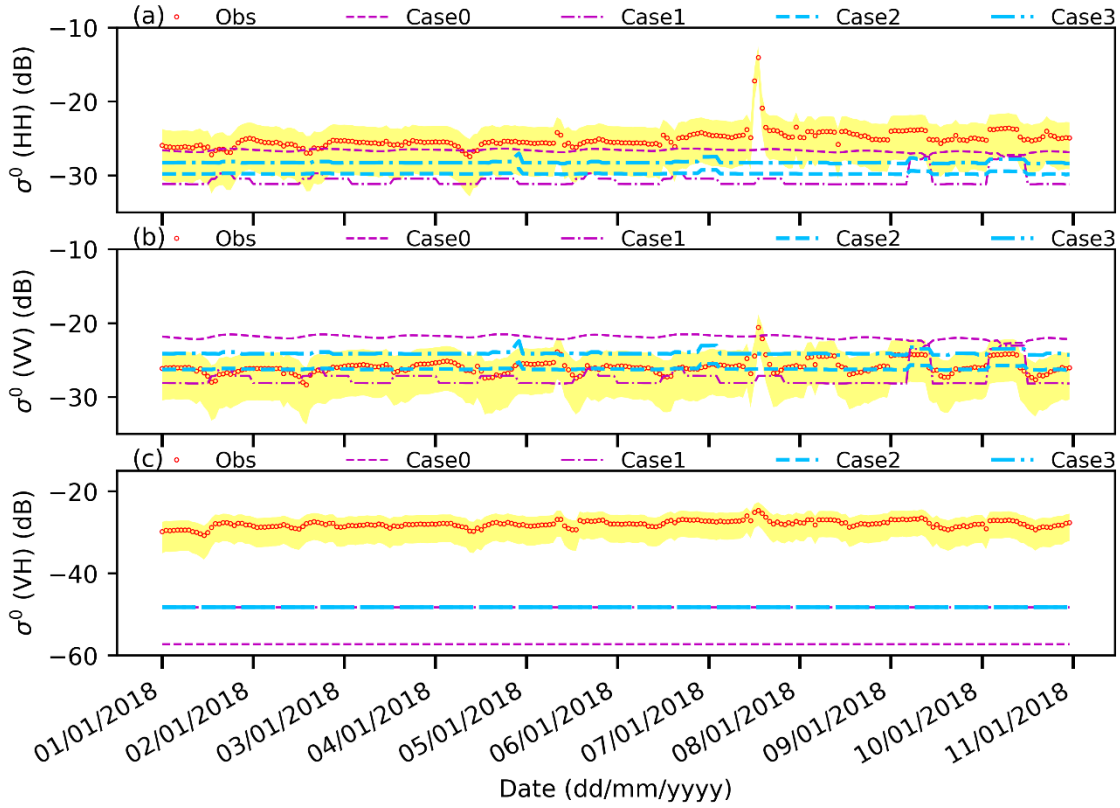


Figure S26 Comparison of  $\sigma_{pq}^0$  at the L-band estimated by four experimental cases to the ELBARA-III observations during the winter period. Case0 refers to the ATS parameterization (Zhao et al., 2021) using soil moisture at 2.5 cm (SM1) and the average dielectric surface with thickness  $b1 = [h/2, h/2 - \log(SM1) * s]$  in the ATS model. Case1 refers to the parameterization using SM1 the same as Case0 and the average dielectric surface with thickness  $b2 = [0, -\log(SM1) * s]$  that represents the shallow surface condition. Case2 refers to the parameterization using the b2 condition and soil moisture at the penetration depth (SM\_pd) of soil temperature (Lv et al., 2018). Case3 refers to the parameterization using SM\_pd and a new boundary of  $b3 = [\text{wavelength}/10, -\log(SM\_pd) * \text{wavelength}/10]$  that considers the wavelength information and the surface condition along the theoretical effective penetration depth of soil moisture (i.e., 1/10 of the wavelength as described in section 1).

Table S2 Statistics of the comparison of  $T_B^P$  at the L-band simulated by the four experimental cases (Figure S8) respectively in the CLAP, to the ground-based observations during the winter period. Bias and RMSE are in the unit of K.

Scheme	H		V	
	Bias	RMSE	Bias	RMSE
Case0	48	49	26	26
Case1	-10	16	-13	15
Case2	-2	5	-9	9
Case3	19	20	4	5

\* Case0 refers to the parameterization using soil moisture at 2.5 cm (SM1) and the average dielectric surface with thickness  $b1 = [h/2, h/2 - \log(SM1) * s]$  in the ATS model. Case1 refers to the parameterization using SM1 the same as Case0 and the average dielectric surface with thickness  $b2 = [0, -\log(SM1) * s]$  that represents the shallow surface condition. Case2 refers to the parameterization using the b2 condition and soil moisture at the penetration depth (SM\_pd) of soil temperature (Lv et al., 2018). Case3 refers to the parameterization using SM\_pd and a new boundary of  $b3 = [\text{wavelength}/10, -\log(SM\_pd) * \text{wavelength}/10]$  that considers the wavelength information and the surface condition along the theoretical effective penetration depth of soil moisture (i.e., 1/10 of the wavelength as described in section 1).

Table S3 Statistics of the comparison of  $\sigma_{pq}^0$  at the L-band simulated by the four experimental cases (Figure S8) respectively in the CLAP, to the ground-based observations during the winter period. Bias and RMSE are in the unit of dB.

Scheme	HH		VV	
	Bias	RMSE	Bias	RMSE
Case0	1.5	2	-4	4.2
Case1	5.5	5.7	1.5	2
Case2	4.6	4.8	0.2	0.9
Case3	3.1	3.3	-1.9	2.1

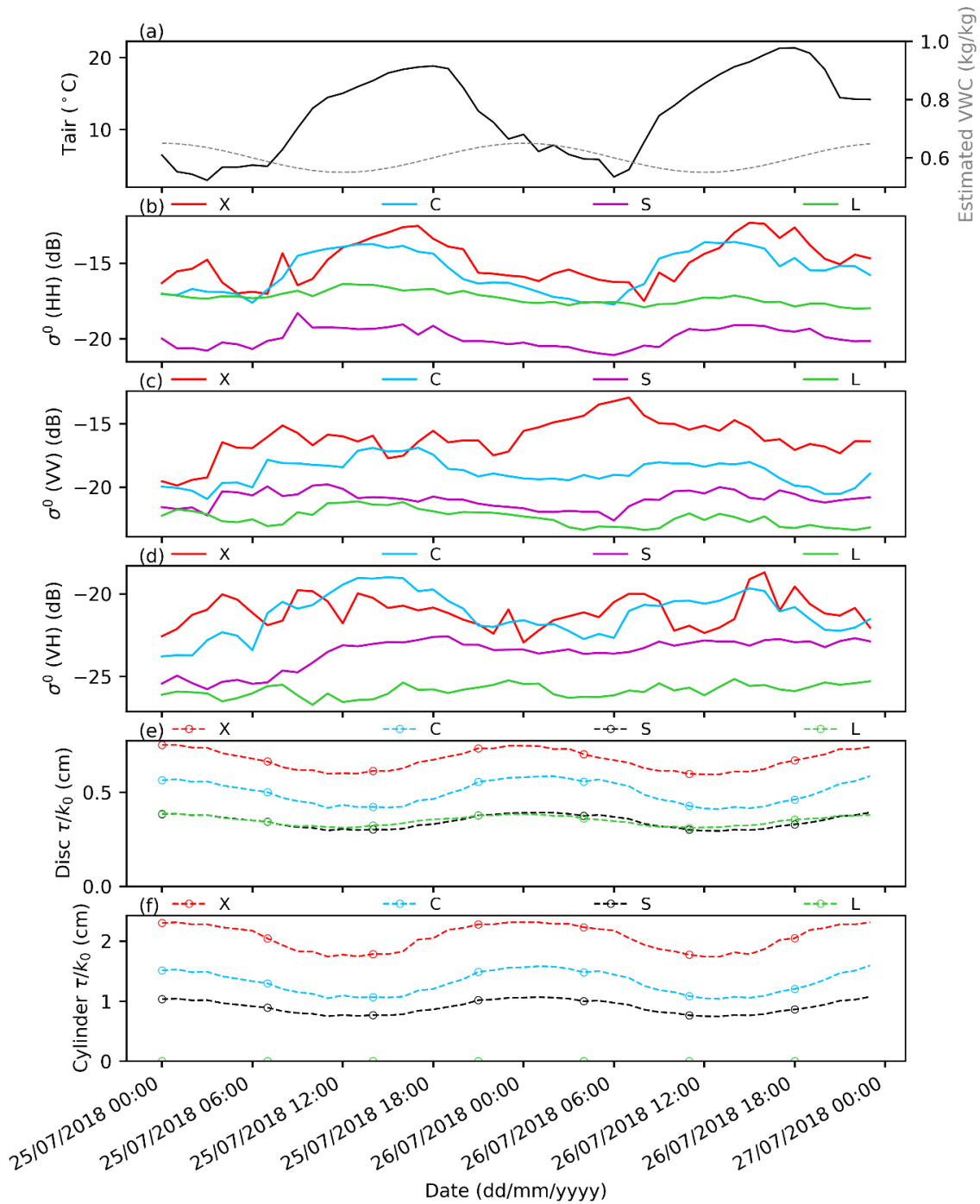


Figure S27 Plot of wavenumber ( $k_0$ ) normalized optical depth ( $\tau$ ) estimated by the disc and cylinder parameterizations respectively, environmental variables and the scatterometer measured  $\sigma^0$ . Tair represents air temperature (°C) at 2 m.

## Reference

Hofste, J. G., van der Velde, R., Wen, J., Wang, X., Wang, Z., Zheng, D., van der Tol, C., and Su, Z.: Year-long, broad-band, microwave backscatter observations of an alpine meadow over the Tibetan Plateau with a ground-based scatterometer, *Earth Syst. Sci. Data*, 13, 2819-2856, <https://doi.org/10.5194/essd-13-2819-2021>, 2021.

Lv, S., Zeng, Y., Wen, J., Zhao, H., and Su, Z.: Estimation of Penetration Depth from Soil Effective Temperature in Microwave Radiometry, *Remote. Sens.*, 10, 1-19, <https://doi.org/10.3390/rs10040519>, 2018.

Zhao, H., Zeng, Y., Wen, J., Wang, X., Wang, Z., Meng, X., and Su, Z.: An Air-to-Soil Transition Model for Discrete Scattering-Emission Modelling at L-Band, *J. Remote Sens.*, 2021, 1-20, <https://doi.org/10.34133/2021/3962350>, 2021.